

Three-dimensional physical simulation and optimization of water injection of a multi-well fractured-vuggy unit

Ji-Rui Hou^{1,2,3} · Ze-Yu Zheng^{1,2,3} · Zhao-Jie Song^{1,2,3} · Min Luo^{1,2,3} · Hai-Bo Li^{1,2,3} · Li Zhang^{1,2,3} · Deng-Yu Yuan^{1,2,3}

Received: 3 December 2014 / Published online: 16 March 2016
© The Author(s) 2016. This article is published with open access at Springerlink.com

Abstract With complex fractured-vuggy heterogeneous structures, water has to be injected to facilitate oil production. However, the effect of different water injection modes on oil recovery varies. The limitation of existing numerical simulation methods in representing fractured-vuggy carbonate reservoirs makes numerical simulation difficult to characterize the fluid flow in these reservoirs. In this paper, based on a geological example unit in the Tahe Oilfield, a three-dimensional physical model was designed and constructed to simulate fluid flow in a fractured-vuggy reservoir according to similarity criteria. The model was validated by simulating a bottom water drive reservoir, and then subsequent water injection modes were optimized. These were continuous (constant rate), intermittent, and pulsed injection of water. Experimental results reveal that due to the unbalanced formation pressure caused by pulsed water injection, the swept volume was expanded and consequently the highest oil recovery increment was achieved. Similar to continuous water injection, intermittent injection was influenced by factors including the connectivity of the fractured-vuggy reservoir, well depth, and the injection–production relationship, which led to a relative low oil recovery. This study may provide a

constructive guide to field production and for the development of the commercial numerical models specialized for fractured-vuggy carbonate reservoirs.

Keywords Multi-well fractured-vuggy unit · Three-dimensional physical model · Similarity criteria · Bottom water drive · Optimization of water injection mode

1 Introduction

Carbonate reservoirs are the important sources of hydrocarbons, accounting for half of world's oil and gas reserves (Li and Chen 2013; Yousef et al. 2014). The Tahe Oilfield is the largest oilfield found in the Paleozoic marine carbonates in China (Li et al. 2014a). The successful exploitation of this oilfield can significantly reduce the crisis of the hydrocarbon shortage in China.

The Tahe Oilfield is located in the middle of the South Tarim Uplift in the Tarim Basin, China, with an area of 2400 km² (Li et al. 2014b). The Ordovician reservoir in the Tahe Oilfield is an example of fractured-vuggy carbonate reservoirs (Li 2013). The reservoir space is complicated because of the co-existence of vugs, fractures, and large caves in these reservoirs (Xu et al. 2012). Large caves serve as the main storage space, while fractures act as the primary flow paths with only a little oil accumulated in them (Lv et al. 2011; Zhang and Wang 2004). On the other hand, the carbonate matrix exhibits ultra-low permeability and almost no storage ability. Therefore, a fractured-vuggy unit is considered as the basic production unit during the exploitation of these carbonate reservoirs (Yi et al. 2011; Rong et al. 2013). This type of reservoir is characterized by serious heterogeneity, random distribution, and complex co-location of fractures and vugs, and various filling types

✉ Ze-Yu Zheng
zhengzeyu890808@outlook.com

¹ Research Institute of Enhanced Oil Recovery, China University of Petroleum, Beijing 102249, China

² Key Laboratory of Marine Facies, Sinopec, Beijing 102249, China

³ Key Laboratory of Petroleum Engineering, Ministry of Education, Beijing 102249, China

and filling percentages of storage space. Therefore, fractured-vuggy carbonate reservoirs are very complex with multiple oil–water systems and the existence of bottom water, which makes hydrocarbon production difficult (Popov et al. 2009; Lucia et al. 2003).

And so far, in most of the numerical simulations of fractured-vuggy carbonate reservoirs, this type of reservoir is taken as equivalent to sandstone reservoirs, e.g., CMG, Eclipse (Presho et al. 2011; Wu et al. 2011; Guo et al. 2012). A commercial numerical simulator specialized for fractured-vuggy carbonate reservoirs has not yet been developed. Consequently, fundamental experimental research is required to provide a theoretical foundation for numerical simulations.

Previous research has been conducted on fractured-vuggy reservoirs through physical simulations (Cruz et al. 2001; Zheng et al. 2010; Zhang et al. 2011; Jia et al. 2013; Xu et al. 2013). Cruz et al. (2001) performed water-displacing oil experiments using a two-dimensional vuggy fractured porous cell, took photographs of the water front, measured the flow area corresponding to oil and water, and finally developed a theoretical model based on the experimental results. Zheng et al. (2010) designed and constructed a cylindrical core model, according to actual conditions of a fractured-vuggy carbonate reservoir. Water-displacing oil experiments were conducted and it is found that oil recovery, water cut, and water breakthrough were significantly impacted by fractured-vuggy structures. Zhang et al. (2011)

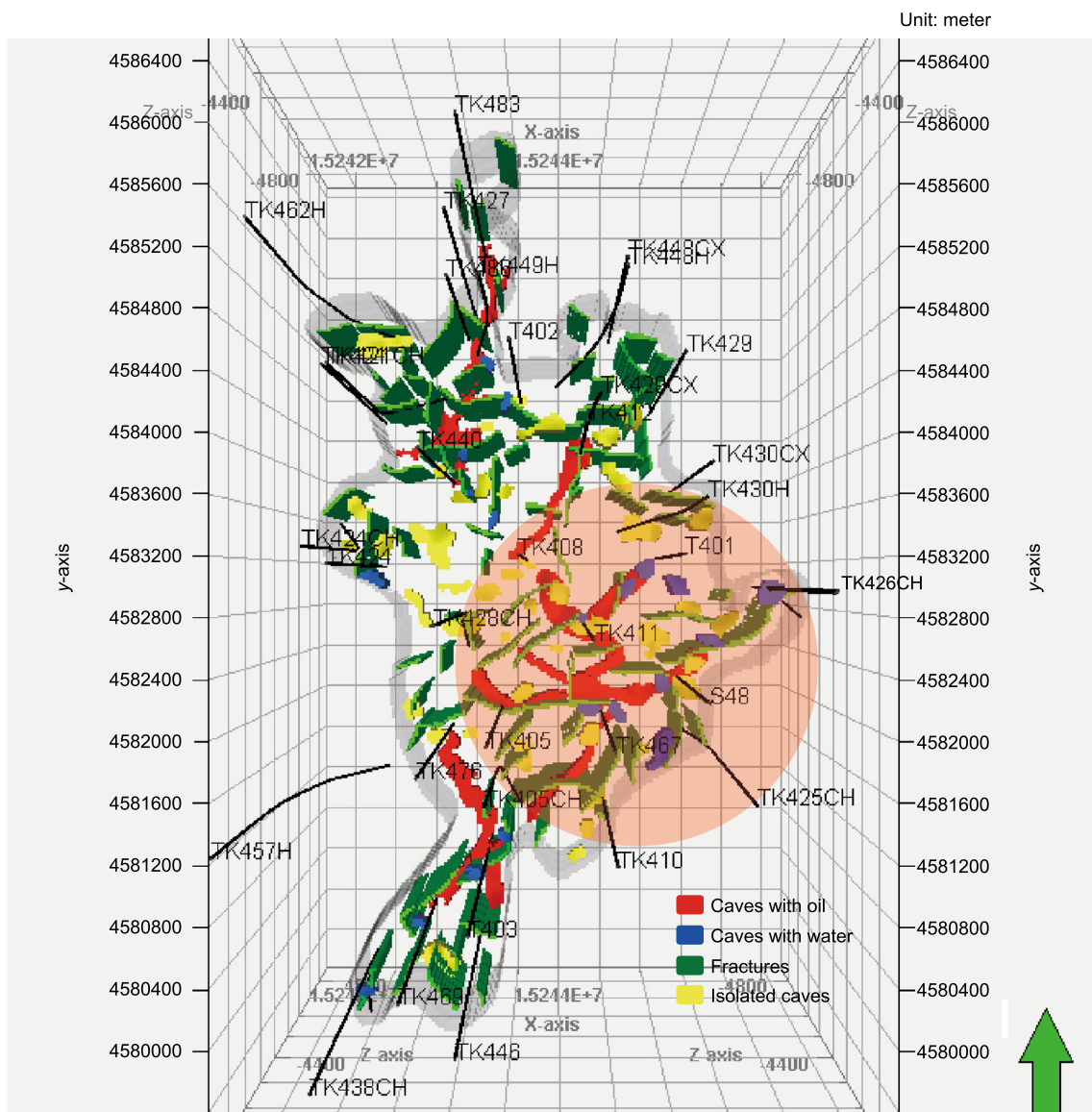


Fig. 1 Geological conditions of the example reservoir

built a single-phase fluid flow pattern in fractured-vuggy media with different vug densities, and concluded that with an increase in vug density, the pressure gradient at the same velocity declined and the critical velocity increased. However, due to the limitations of dimensionality, similarity design, and other factors, three-dimensional fluid flow in

porous media is difficult to simulate reliably in these models. In this paper, a three-dimensional physical model is designed and built based on a geological example unit in the Tahe Oilfield and similarity criteria. Bottom water drive is conducted to validate the 3D physical model according to well history and then the optimization of water injection

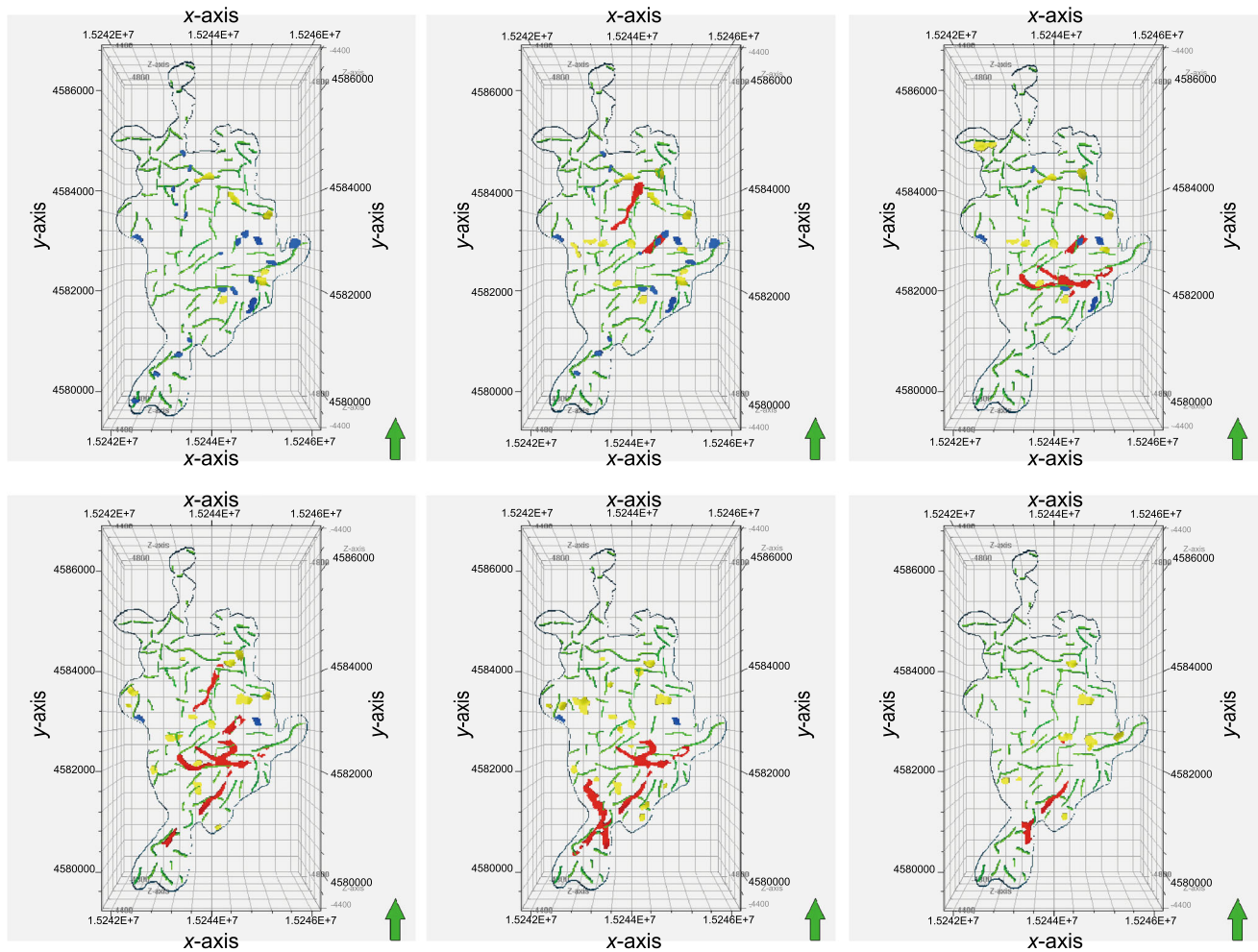


Fig. 2 Longitudinal sections of the reservoir

Table 1 Production histories of 5 wells with bottom water drive in the S48 unit

Well	Production date	Production duration, y	Crude output, 10 ⁴ m ³	Liquid output, 10 ⁴ m ³	Annual liquid output, 10 ⁴ m ³ /y
S48	1997	12	80.04	94.02	7.83
T401	1998	11	50.17	63.24	5.75
TK411	1999	10	12.87	18.61	1.86
Tk426CH	2000	9	2.650	10.73	1.19
TK467	2002	7	9.714	14.21	2.03

Table 2 Annual data of the S48 unit with bottom water drive

Year	Annual liquid output, 10^4 m^3	Daily liquid output, m^3/d
1997*	2.889	481.4
1998	17.36	475.7
1999	31.13	852.9
2000	41.50	1137
2001	29.33	803.5
2002	23.40	373.2
2003	12.20	334.2
2004	9.340	255.9
2005	9.328	255.6
2006	10.04	275.0
2007	11.91	326.4
2008	14.78	404.9

* The wells only produced for two months in 1997

modes is performed by means of continuous, intermittent, and pulsed injection of water.

The experimental results may provide an insight into the later production with water injection and numerical simulations of fractured-vuggy carbonate reservoirs.

2 Geological example and well history

2.1 Example reservoir

Five wells, S48, T401, TK411, TK426CH, and TK467, in the S48 unit in the Tahe Oilfield were chosen as examples to design a 3D physical model, as shown in Fig. 1. The red part in Fig. 1 indicates the area of influence of the chosen well groups. The longitudinal sections of the reservoir are presented in Fig. 2.

Table 3 Physical parameters and dimensions related to oil and water two-phase flow in a multi-well fractured-vuggy unit

Category	Number	Physical parameter	Symbol	Dimension
Basic physical parameter	1	Quality	m	M
	2	Time	t	T
	3	Length	l	L
Dimensional parameter	4	Oil flow rate	u_o	LT^{-1}
	5	Water flow rate	u_w	LT^{-1}
	6	Oil density	ρ_o	ML^{-3}
	7	Water density	ρ_w	ML^{-3}
	8	Oil viscosity	μ_o	$\text{ML}^{-1}\text{T}^{-1}$
	9	Water viscosity	μ_w	$\text{ML}^{-1}\text{T}^{-1}$
	10	Volume flow rate of oil	Q_o	L^3T^{-1}
	11	Volume flow rate of water	Q_w	L^3T^{-1}
	12	Injection pressure	P	$\text{ML}^{-1}\text{T}^{-2}$
	13	Acceleration of gravity	g	LT^{-2}
	14	Fracture permeability	K_f	L^2
	15	Cave height	H	L
	16	Fracture aperture	B	L
	17	Cave diameter	d	L
	18	Fracture density	n_f	L^{-1}
	Dimensionless parameter	19	Cave density	n_v
20		Fluid compressibility	C_L	LT^2M^{-1}
21		Total compressibility	C_t	LT^2M^{-1}
22		Fracture porosity	Φ_f	
23		Cavernous porosity	Φ_v	
24		Oil relative permeability	K_{ro}	
25		Water relative permeability	K_{rw}	
26		Oil saturation	S_o	
27		Water saturation	S_w	
28		Pseudo coordination number	ξ	
29		Filling percentage	η	

2.2 Well history

A 3D physical model was constructed based on the example of the geology of the S48 unit. Bottom water drive was employed in the S48 unit in the early stage of production. The physical model was required to be similar to actual reservoir conditions so that experimental results are as reliable as possible. Hence, it is imperative to understand and analyze the practical production situations during bottom water drive. Tables 1 and 2 depict well history information of the S48 unit. According to well history and other information reported earlier (Zhu et al. 2009; Hu et al. 2013), an oil recovery of 20 %–23 % was obtained at the end of bottom water drive in this unit.

3 Physical model design and fabrication

3.1 Similarity design

According to previous studies of physical simulation (Elkaddifi et al. 2008; Zhang et al. 2008; Bünger and Herwig 2009; Zuta and Fjelde 2011; Wang et al. 2014), some similarity criteria, such as geometric similarity, kinematic similarity, dynamic similarity, and characteristic parameter similarity, were adopted to insure the similarity between the physical model and the geological example.

However, it was impossible to achieve similarity of all parameters. Thus, a dimensional analysis method was introduced to simplify the similarity criterions.

The characteristics of oil and water two-phase flow in a multi-well fractured-vuggy unit should be taken into account and relevant physical parameters were considered as illustrated in Table 3.

According to Buckingham’s pi-theorem (Haftkhani and Arabi 2013), ρ , u , and l were chosen as basic parameters, and the physical parameters with the same dimensions were classified as a group. The similarity criterion group is obtained as shown in Table 4.

For a specific flow model, the flow field in the physical model is generally similar to that in the actual reservoir when some main similarity criteria are achieved (Kang and Tang. 2014; Nam et al. 2014). The ratio of the cave diameter to the diameter of the area of influence was chosen as a criterion for geometric similarity. Since the bottom water drive is required to be simulated, the liquid production rate and production duration should be similar to actual situations, so π_6 and π_7 in Table 4 were chosen as kinematic similarity criteria. The Reynolds number should be considered when dynamic similarity is discussed. Meanwhile, the ratio of pressure to gravity that influences the fluid distribution in displacement processes needed to be considered. In addition, the physical model should comply with the similarity theorem on some characteristic parameters, such as pseudo coordination number and

Table 4 Similarity criterion group of the multi-well fractured-vuggy unit

Geometric similarity	Kinematic similarity	Dynamic similarity	Characteristic parameter similarity
$\pi_1 = d/l$	$\pi_6 = Q/(ul^2)$	$\pi_8 = \mu/(\rho ul)$	$\pi_{11} = \xi$
$\pi_2 = B/l$	$\pi_7 = t/ul$	$\pi_9 = P/(\rho u^2)$	$\pi_{12} = \eta$
$\pi_3 = K_f/l^2$	–	$\pi_{10} = gl/u^2$	$\pi_{13} = n_t l$
$\pi_4 = \Phi_f$	–	–	$\pi_{14} = n_v l^2$
$\pi_5 = \Phi_v$	–	–	–

Table 5 Comparison of parameters of the example reservoir and the physical model

Parameter	Example reservoir	Physical model	Similarity coefficient
Cave diameter	5–25 m	3–12 cm	166.7–200.0
Differential pressure	2–14 MPa	10–60 kPa	200.0–233.3
Oil viscosity	19.7–28.5 mPa s	65 mPa s	0.3038–0.4377
Oil density	0.92 g/cm ³	0.8 g/cm ³	1.150
Acceleration of gravity	9.8 m/s ²	9.8 m/s ²	1.000
Fracture density	3–50/m	50/m	0.05880–1.000
Fracture aperture	0.5–5 mm	2–4.5 mm	0.2500–1.110
Fluid flow velocity	30–135 m/d	0.022–0.152 m/s	0.001585–0.001903
Liquid production rate	255.6–1137 m ³ /d	4–10 mL/min	44.37–78.97
Production duration	1 year	5 min	1.051 × 10 ⁵
Filling percentage	0 %–100 %	0 %–100 %	1
Coordination number	1–5	1–5	1

filling percentage. Since it is difficult for a physical model to satisfy multiple similarity criteria simultaneously, the Reynolds number should always be given priority.

The index of the similarity criteria was calculated according to similarity coefficients. A similarity coefficient is the ratio of field parameters to model parameters. If a certain index of the similarity criterion is 1, this model parameter is fully compliant with the field parameter. Based on the discussion mentioned above, the similarity

coefficients and similarity indices of the physical model are obtained as shown in Tables 5 and 6.

3.2 Model fabrication

Longitudinal sections of the example reservoir were divided into six layers, as shown in Fig. 3. Caves and fractures were carved in each core based on the example reservoir. After that, these six cores were bonded together in a given

Table 6 Similarity indices of the physical model

Similarity condition	Similarity criterion	Physical meaning	Source	Similarity index
Geometric similarity	d/l	The ratio of the cave diameter to the diameter of the area of influence	$\pi 1$	1
Kinematic similarity	$\rho u l / \mu$	Reynolds number (the ratio of inertia force to viscous force)	$1/\pi 8$	1
	$P/(\rho g l)$	The ratio of the injection pressure to gravity	$\pi 9 / \pi 10$	1.01–1.04
Dynamic similarity	$Q/(u l^2)$	The ratio of the liquid production rate to the injection rate	$\pi 6$	1.01–1.04
	$t/u l$	The ratio of the production duration to the injection duration	$\pi 7$	1
Characteristic parameter similarity	ξ	Pseudo coordination number	$\pi 11$	1
	η	Filling percentage	$\pi 12$	1

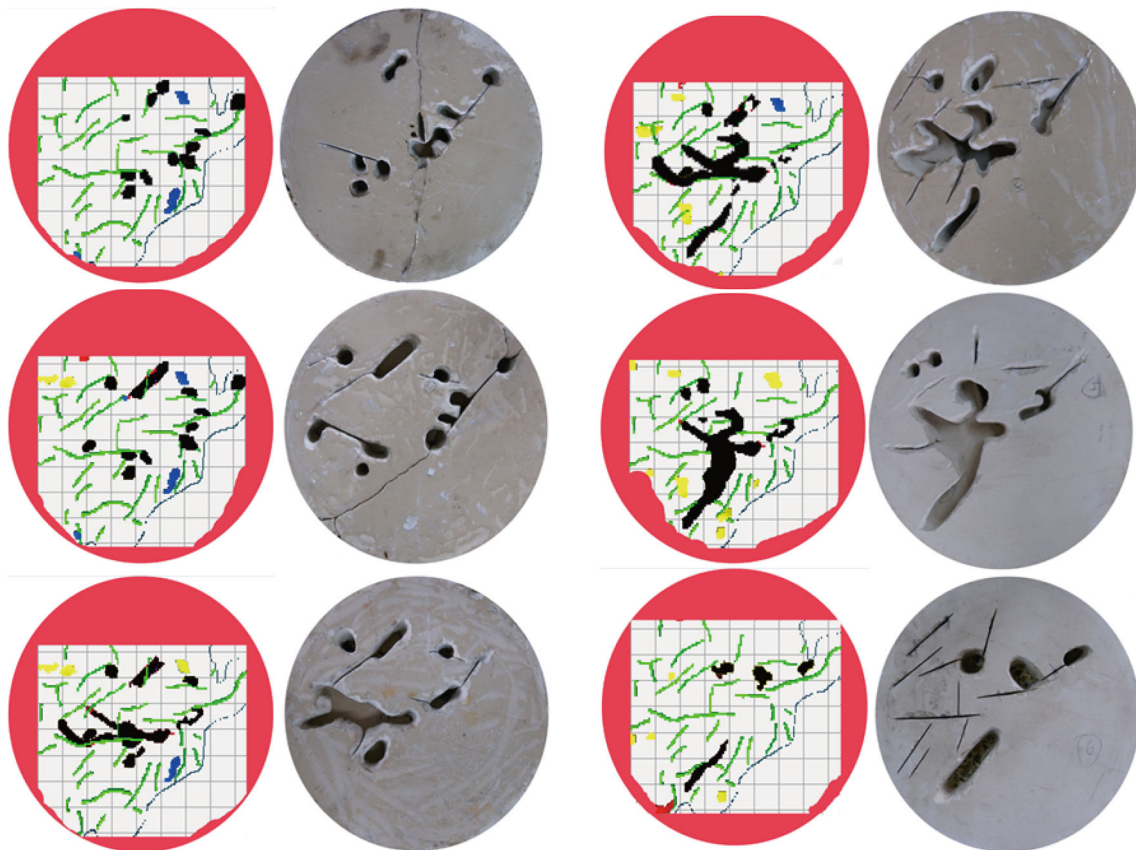


Fig. 3 Comparison of the fractured-vuggy structures between the physical model and the real core for each layer

order. The flow paths of the bottom water and well locations were designed, and a three-dimensional model was fabricated. Finally, the model was put into a cylindrical mold and it was encapsulated and fixated with epoxy resin, as presented in Fig. 4. More details of the physical model were described elsewhere (Hou et al. 2014).

3.3 Fracture and cave structures and well locations

A fractured-vuggy unit with a complex structure was formed in a 3D space, as shown in Fig. 5. In order to make the model similar to the actual formation, caves and fractures were filled with gravel in a certain order of completely filled, half-filled, and unfilled from bottom to top.

Five wells were drilled in the model according to the designed depths and locations. These wells were drilled in different reservoir bodies, i.e., cave and fracture. Wells were divided into two types: one is cave-well which is marked by “D” and the other is fracture-well marked by “L.” Figure 6 illustrates the well locations and Table 7 shows the well parameters.

4 Experimental

4.1 Experimental apparatus and materials

The experimental apparatus (Fig. 7) included a 3D physical model, three intermediate containers, two water injection pumps with a pressure range of 0–30 MPa and a flow rate range of 0.01–10.00 mL/min, several pressure transducers, some six-port valves, etc.

The simulated oil used was a mixture of kerosene and dehydrated crude, with a viscosity of 65 mPa s at 25 °C.

The simulated formation water used had a salinity of 2×10^5 mg/L.

4.2 Experimental procedures

The experimental procedures are as follows:

- (1) The physical model was evacuated and then saturated with the simulated formation water at 10 mL/min from pipelines 6 in Fig. 7. The total volume of water injected into the model was measured to calculate the pore volume (PV) of fractures and caves in the physical model.
- (2) The model was flooded with the simulated oil at 10 mL/min from pipelines 13 from the top of the model and the water was drained from pipelines 6. This was continued until no more water was drained.

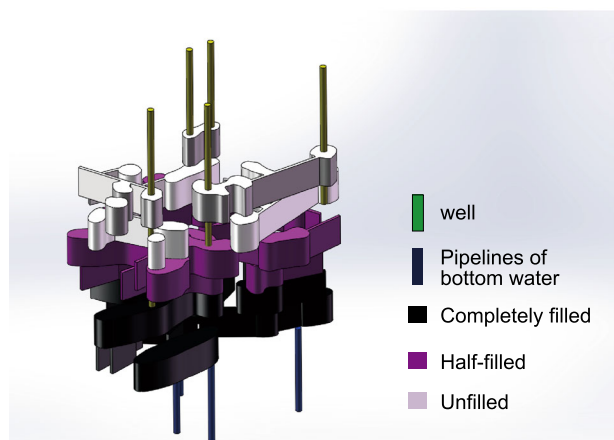


Fig. 5 Fractured-vuggy structure inside the three-dimensional physical model



Fig. 4 The real core after combination

The total volume of water displaced from the model was measured, and the initial oil saturation and the water saturation of the model were then calculated.

- (3) As shown in Fig. 7a, the simulated formation water was continuously introduced into the bottom of the model; the water injection rate was varied to simulate the stage of depletion of a bottom water drive reservoir. The initial water injection rate was set at 10 mL/min and then decreased to 6 mL/min after 15 min, and to 4 mL/min after another 5 min. The injection rate was kept at 4 mL/min until a 98 % water cut was reached in one of these five production wells. The oil and water production rate was monitored to calculate oil recovery and periodic water cut. Five wells were put into production in the order D1, D2, L2, L3, and L1, as depicted in Table 8.
- (4) During the bottom water drive, the water cut of Well L1 reached 98 % first. This well was then switched to be an injection well. After the bottom water drive, the experimental apparatus was set up as shown in Fig. 7b. Water was subsequently introduced into the model through Well L1; water injection rates at

different waterflood projects are listed in Table 9. Each production well was shut in once its water cut reached 98 %. The experiment was stopped when the four production wells were all shut in. The oil and water production rates were monitored to calculate the oil recovery and periodic water cut.

5 Experimental results and discussion

5.1 Performance of the bottom water drive model

The production performance of the bottom water drive model constructed in this study is shown in Fig. 8. The oil recoveries of five production wells increased slowly at this stage, i.e., the oil production rate declined, and the water cut of fluids produced from Well L1 increased as the bottom water energy was depleted.

Water breakthrough occurred immediately in Well L1 and its water cut rose rapidly after this well was put into production. This is because Well L1 was the deepest well (Table 7). Experimental results are consistent with actual production situation. The experiment was stopped when the water cut of fluids produced from Well L1 reached 98 %. The total oil recovery was about 22.1 %, which is in agreement with the actual oil recovery in the S48 unit. Thus, experimental results verified that the 3D physical model had similarity to the example reservoir (S48 unit).

5.2 Optimization of water injection schemes

Due to the viscosity difference between water and oil in the water/oil interface, the flow rate of water is higher than that of oil under the same differential pressure. When the differential pressure is high enough, water can probably flow vertically upward. Therefore, a conical water/oil interface was formed, which is known as bottom water coning (Xiao et al. 2010).

By injecting water into the reservoir through a drowned well to supply energy, bottom water coning could be mitigated and the intrusive water phase could be suppressed toward the opposite direction (Lu et al. 2009). However, different water injection modes exert different effects on

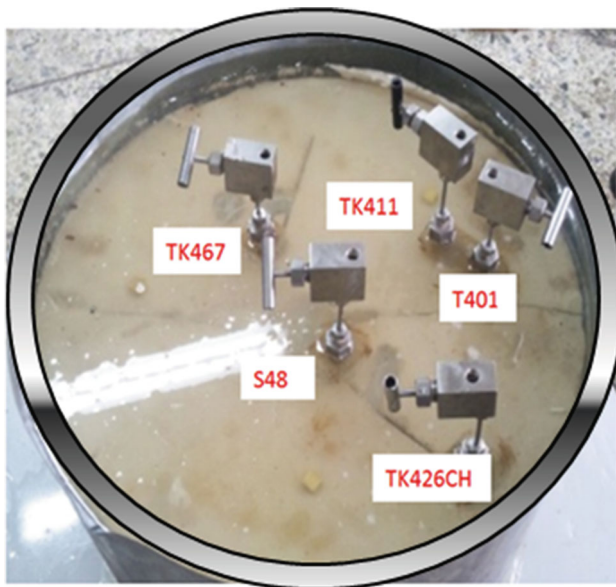


Fig. 6 Well locations in the three-dimensional physical model

Table 7 Well parameters of the models

Number	Well	Well depth, cm	Well type	Filling percentage
D1	S48	14.8	Cave-well	Half-filled
D2	T401	12.2	Cave-well	Half-filled
L1	TK467	18.0	Fracture-well	Completely filled
L2	TK411	17.8	Fracture-well	Completely filled
L3	TK426CH	9.2	Fracture-well	Unfilled

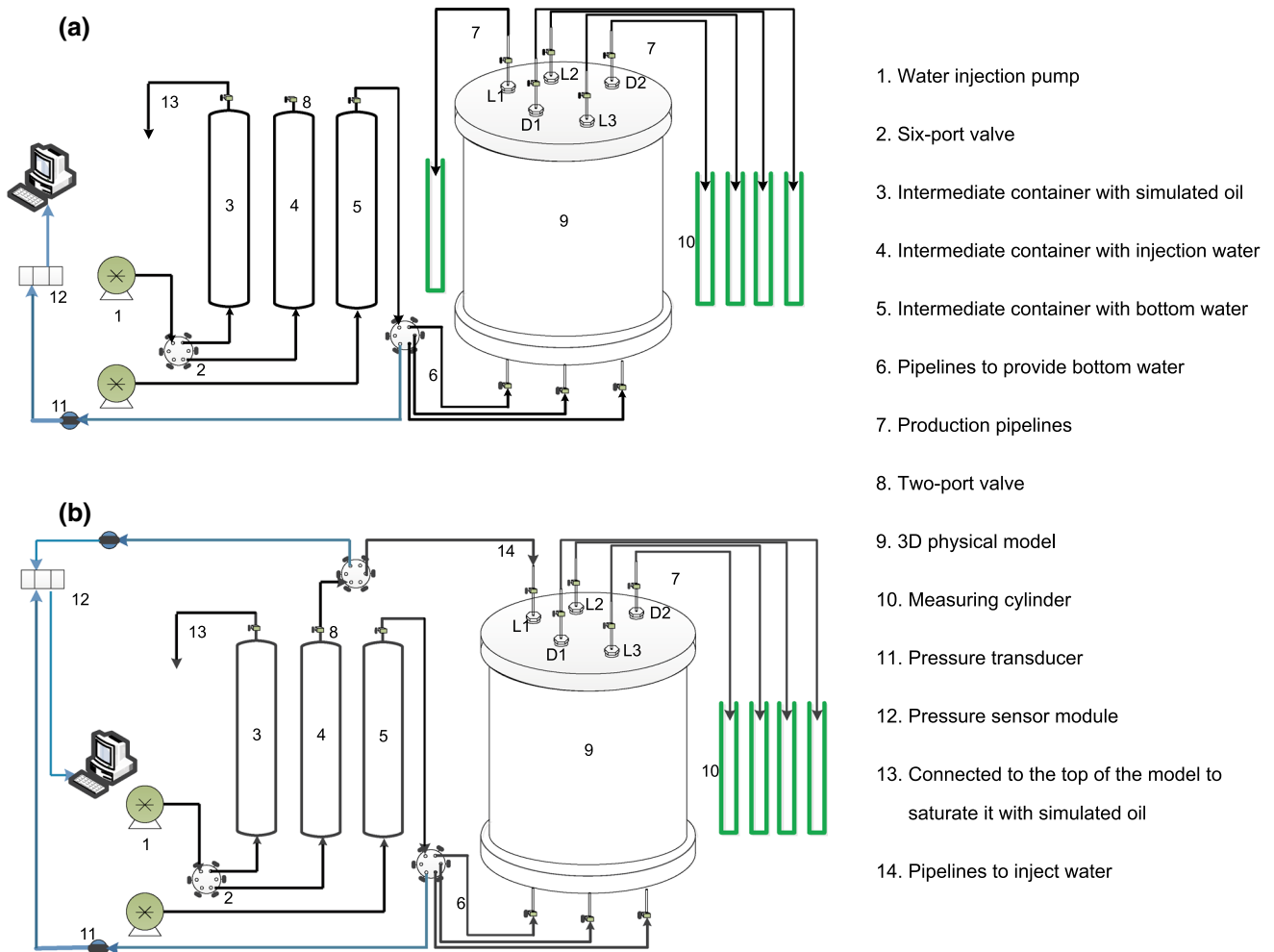


Fig. 7 Schematic diagram of experimental setups for the bottom water drive (a) and the water injection mode optimization (b)

Table 8 Well startup order in the bottom water drive model

Timing, min	Well startup order
0	D1
5	D2
10	L2
15	L3
25	L1

mitigating water coning. Therefore, the objective of the following work is to optimize water injection modes, including continuous injection (constant rate), intermittent injection, and pulsed injection of water.

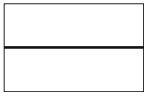

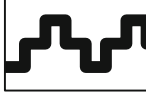
5.2.1 Overall effect of subsequent water injection

Figures 9 and 10 show the dynamic curves of oil recovery and differential pressure for three water injection schemes, respectively.

No matter which water injection scheme was performed, the oil recovery increased substantially at the beginning and then continued to rise smoothly until the oil recovery became relatively stable as no more oil was being produced. The highest oil recovery of 47.0 % was obtained after pulsed injection of water. Similar oil recoveries, 44.7 % and 44.3 %, respectively, were obtained after continuous and intermittent injection of water.

The differential pressure fluctuated significantly during intermittent and pulsed injection of water (Fig. 10). The amplitude of pressure fluctuations was relatively large when water was intermittently injected into Well L1 every 25 min, while the frequency of pressure fluctuations was relatively high during pulsed injection of water. This indicates that unsteady-state water injection, including intermittent injection and pulsed injection, might promote the instability of fluid flow rate, flow direction, and pressure distribution in the model. In this way, the water displacement efficiency was improved. However, the

Table 9 Experimental schemes for optimizing water injection

Scheme	Injection rate of bottom water, mL/min	Subsequent water injection		Diagrams of injection rate
		Injection scheme	Injection rate	
A	4	Continuous injection	4 mL/min	
B	4	Intermittent injection	8 mL/min for 25 min and 0 mL/min for another 25 min in one cycle	
C	4	Pulsed injection	2 mL/min for 15 min, 4 mL/min for 15 min, 6 mL/min for 15 min, and 4 mL/min for 15 min in one cycle	

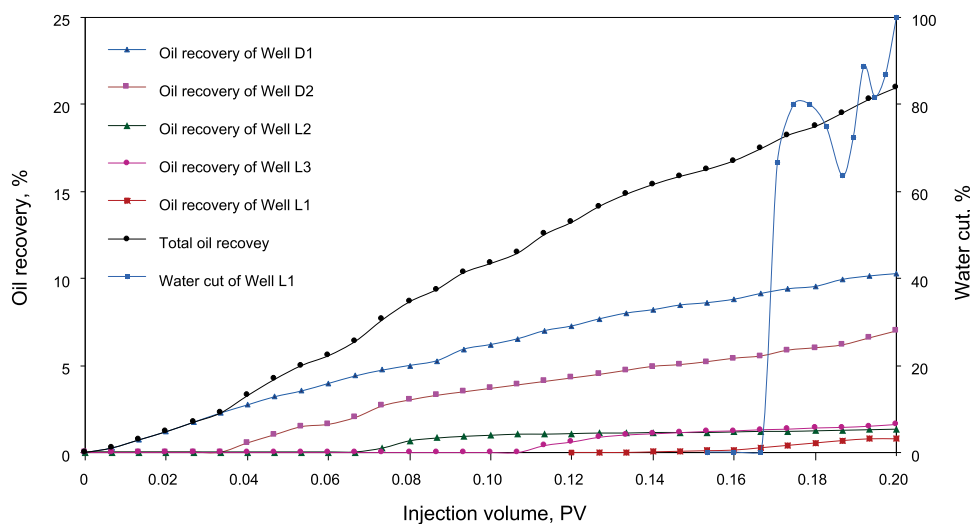


Fig. 8 Production performance of the bottom water drive at the depletion stage

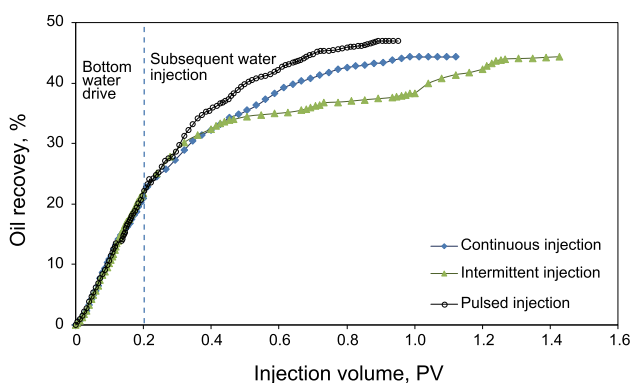


Fig. 9 Dynamic oil recovery curve

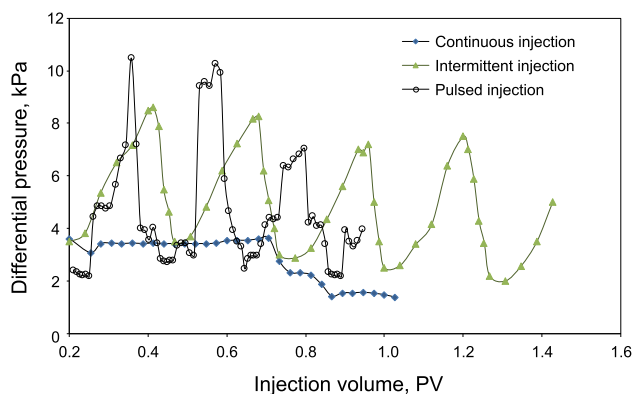


Fig. 10 Injection pressure during water injection

displacement efficiency of intermittent injection was not as good as expected. This is due to the serious heterogeneity and the complex structure of fractures and caves in the fractured-vuggy reservoir model.

5.2.2 Production performance at the subsequent water injection stage

Figures 11, 12, 13, and 14 present the oil recovery and water cut of four production wells at the subsequent water injection stage, respectively.

Well L2 was the nearest to the injection well L1, and its well depth was similar to Well L1. Therefore, water breakthrough occurred immediately in Well L2 when the water was injected into Well L1. Correspondingly, the water cut of Well L2 increased to 100 % rapidly. The incremental oil recovery was only about 0.1 %–0.2 %.

Because Well D1 was drilled deeply into a cave that was near to injection well L1, water breakthrough occurred easily during subsequent water injection. The final oil recovery of Well D1 after intermittent injection was the highest among these three water injection modes. During intermittent injection, the injection pressure of Well D1 was high enough to suppress bottom water coning. Therefore, the oil/water co-production duration of Well D1 was long and its oil recovery was relative high. However, the incremental oil recovery was still at a low level, less

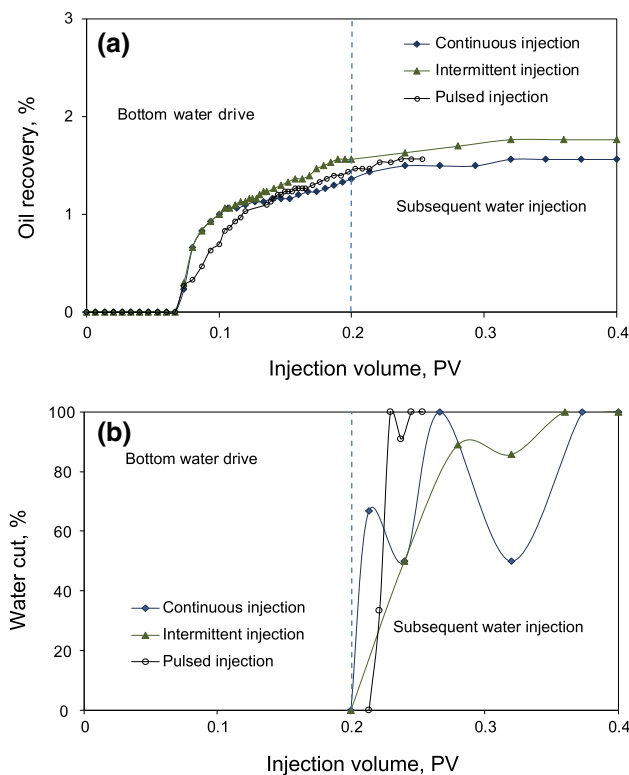


Fig. 11 Dynamic curves of oil recovery and water cut of Well L2

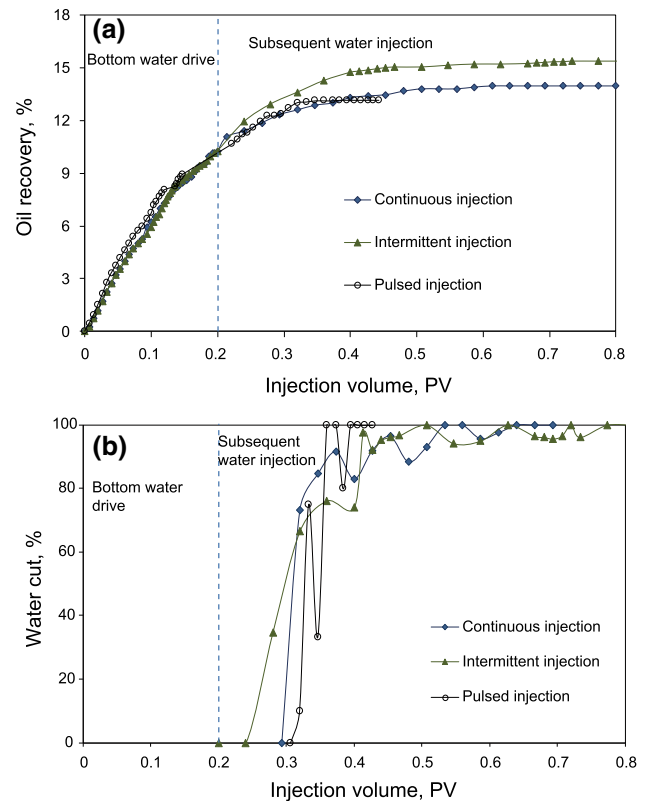


Fig. 12 Dynamic curves of oil recovery and water cut of Well D1

than 5.5 %. All these phenomena can be attributed to the well location, well depth, and the early water breakthrough.

Well D2 was comparatively far from Well L1 and the gravity effect in this well was relatively strong due to a bottom cave. The injection pressure was very low and only supplied bottom water energy during continuous water injection. So, the oil recovery of this well was not high after continuous water injection. On the other hand, the advantage of intermittent and pulsed injection of water was apparent. By changing the injection rate, pressure fluctuations were generated. The formation pressure distribution was changed and the oil–water flow was promoted between fractures and caves. In this way, the sweep efficiency and the displacement efficiency were improved.

Well L3 was also comparatively far away from injection well L1. Unlike Well D2, Well L3 was a fracture-well, and the well depth was the shallowest among those five wells. Therefore, the production performance of Well L3 was completely different from others. During intermittent injection, the injection pressure increased rapidly and water breakthrough occurred easily. However, after the water injection ended, water and oil were hard to redistribute due to the high viscosity resistance and slight gravity effect in fractures. This also led to a relative low oil recovery in Well L3 after immediate injection of water. During pulsed

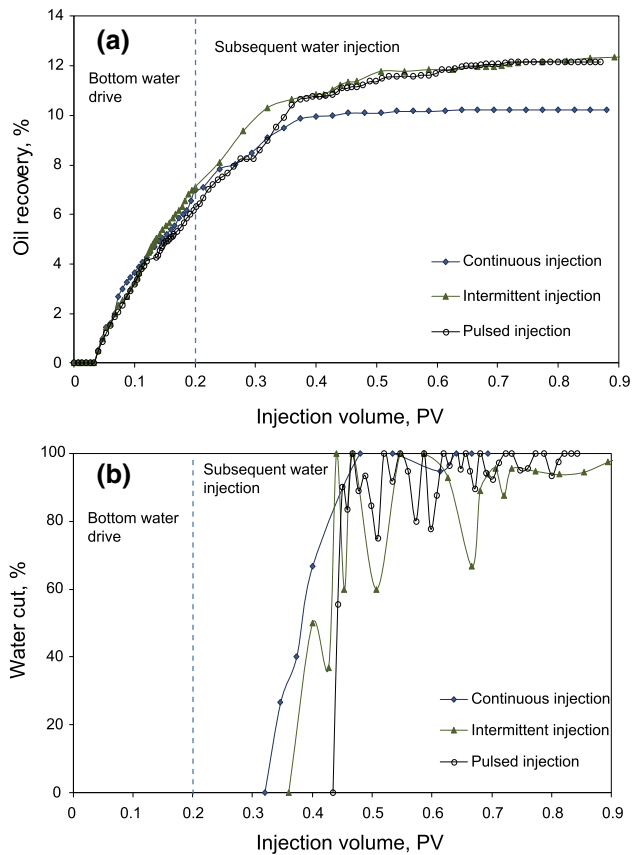


Fig. 13 Dynamic curves of oil recovery and water cut of Well D2

water injection, the high injection rate led to a high pressure increase and caused an early water breakthrough; however, the frequently fluctuated pressure induced a long duration of oil and water co-production, and led to a high final oil recovery.

Due to the complicated fractured-vuggy structure, well location, and well depth, not all the wells exhibited effective response to these three water injection modes. As a whole, the rate of increase of water cut during intermittent and pulsed injection of water was higher than that during continuous water injection. Unsteady-state injection of water indeed enhances water displacement efficiency to some extent compared with steady-state water injection.

6 Conclusions

(1) Based on a multi-well fractured-vuggy geological example unit in the Tahe Oilfield, a large-scale three-dimensional physical model was designed and constructed to simulate the fluid flow according to similarity criteria. Several factors were considered in

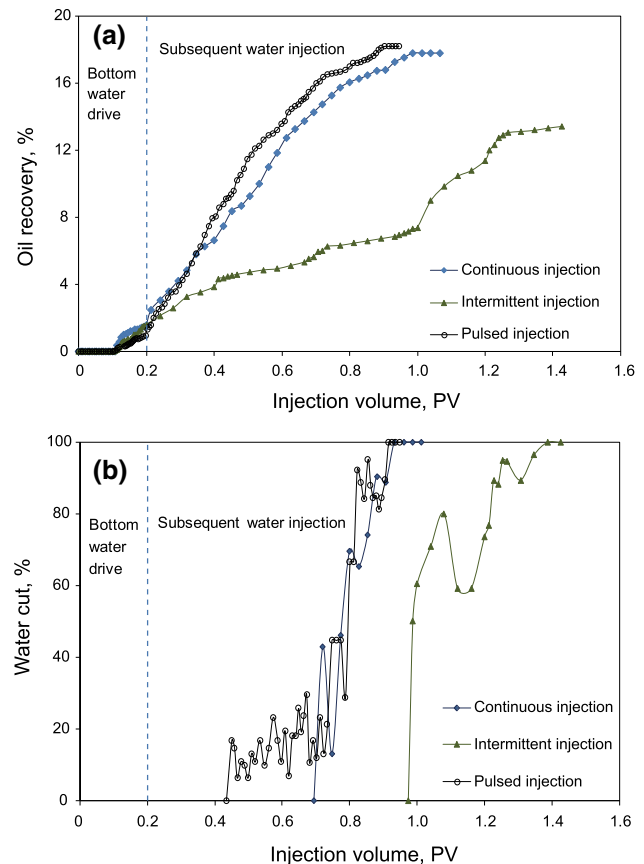


Fig. 14 Dynamic curves of oil recovery and water cut of Well L3

the design, including storage types, filling types, and filling percentages of storage space.

- (2) The depletion production was conducted by changing the bottom water injection rate. Oil recovery of the physical model was similar to that of the field cases, which verified the reliability of the physical model.
- (3) During pulsed injection of water, unbalanced formation pressure was caused, and the swept volume was expanded, and consequently the highest oil recovery increment was achieved. Intermittent injection presented the same effect as pulsed injection. However, similar to continuous injection, intermittent injection was influenced by factors including fractured-vuggy connected manner, well depth, and injection–production relationship. Continuous injection and intermittent injection finally get a comparatively low oil recovery.
- (4) If a well is deep and close to the injection well, water breakthrough may occur earlier and water cut rises more rapidly. Besides, production performances of the fracture-well and the cave-well are completely different due to the difference in gravity effect and viscosity resistance.

Acknowledgments This work was supported by China National Science and Technology Major Project (2011ZX05009-004, 2011ZX05014-003), National Key Basic Research and Development Program (973 Program), China (2011CB201006), and Science Foundation of China University of Petroleum, Beijing (2462014YJRC053).

Open Access This article is distributed under the terms of the Creative Commons Attribution 4.0 International License (<http://creativecommons.org/licenses/by/4.0/>), which permits unrestricted use, distribution, and reproduction in any medium, provided you give appropriate credit to the original author(s) and the source, provide a link to the Creative Commons license, and indicate if changes were made.

References

- Bünger F, Herwig H. An extended similarity theory applied to heated flows in complex geometries. *Zeitschrift für angewandte Mathematik und Physik*. 2009;60(6):1095–111. doi:10.1007/s00033-009-8076-8.
- Cruz HJ, Islas JR, Perez RC, et al. Oil displacement by water in vuggy fractured porous media. In: SPE Latin American and Caribbean petroleum engineering conference, 25–28 March, Buenos Aires, Argentina; 2001. doi:10.2118/69637-MS.
- Elkaddifi K, Shirif E, Ayub M, Henni A. Bottomwater reservoirs: simulation approach. *J Can Pet Technol*. 2008;47(2):38–43. doi:10.2118/08-02-38.
- Guo JC, Nie RS, Jia YL. Dual permeability flow behavior for modeling horizontal well production in fractured-vuggy carbonate reservoirs. *J Hydrol*. 2012;464–5:281–93. doi:10.1016/j.jhydrol.2012.07.021.
- Haftkhani AR, Arabi M. Improve regression-based models for prediction of internal-bond strength of particleboard using Buckingham's pi-theorem. *J For Res*. 2013;24(4):735–40. doi:10.1007/s11676-013-0412-3.
- Hou JR, Li HB, Jiang Y, et al. Macroscopic three-dimensional physical simulation of water flooding in multi-well fracture-cavity unit. *Pet Explor Dev*. 2014;41(6):784–9. doi:10.1016/S1876-3804(14)60093-8.
- Hu XY, Li Y, Wang YQ, et al. Application of the probability method in a 3D geological model for petroleum geological reserves in fractured-cavity carbonate reservoirs: a case of Tahe-IV district, Tahe Oilfield. *Pet Geol Recovery Effic*. 2013;20(4):46–8 (in Chinese).
- Jia YL, Fan XY, Nie RS, et al. Flow modeling of well test analysis for porous-vuggy carbonate reservoirs. *Transp Porous Media*. 2013;97(2):253–79. doi:10.1007/s11242-012-0121-y.
- Kang YY, Tang DB. An approach to product solution generation and evaluation based on the similarity theory and ant colony optimisation. *Int J Comput Integr Manuf*. 2014;27(12):1090–104. doi:10.1080/0951192X.2013.855945.
- Li HB, Hou JR, Li W, et al. Laboratory research on nitrogen foam injection in fracture-vuggy reservoirs for enhanced oil recovery. *Pet Geol Recovery Effic*. 2014a;21(4):93–6 (in Chinese).
- Li JY, Chen XH. A rock-physical modeling method for carbonate reservoirs at seismic scale. *Appl Geophys*. 2013;10(1):1–13. doi:10.1007/s11770-013-0364-6.
- Li M, Lou ZH, Zhu R, et al. Distribution and geochemical characteristics of fluids in Ordovician marine carbonate reservoirs of the Tahe Oilfield. *J Earth Sci*. 2014b;25(3):486–94. doi:10.1007/s12583-014-0453-3.
- Li PL. The development of Ordovician fractured-cavity carbonate reservoirs in the Tahe Oilfield. Beijing: Petroleum Industry Press; 2013. p. 1–6 (in Chinese).
- Lu ZY, Yang M, Dou ZL, et al. Study of geological model of pressure coning by water injection in well group TK440 of Ordovician reservoir in Tahe Oilfield, Tarim Basin, China. *J Mineral Petrol*. 2009;29(4):95–9 (in Chinese).
- Lucia FJ, Kerans C, Jennings JW. Carbonate reservoir characterization. *Soc Pet Eng*. 2003;55(6):70–2. doi:10.2118/82071-MS.
- Lv AM, Yao J, Wang W. Characteristics of oil-water relative permeability and influence mechanism in fractured-vuggy medium. *Proc Eng*. 2011;18:175–83. doi:10.1016/j.proeng.2011.11.028.
- Nam JS, Park YJ, Kim JK, et al. Application of similarity theory to load capacity of gearboxes. *J Mech Sci Technol*. 2014;28(8):3033–40. doi:10.1007/s12206-014-0710-5.
- Popov P, Qin G, Bi LF, et al. Multiphysics and multiscale methods for modeling fluid flow through naturally fractured vuggy carbonate reservoirs. *SPE Eval Eng*. 2009;12(2):218–31. doi:10.2118/105378-PA.
- Presho M, Wo S, Ginting V. Calibrated dual porosity, dual permeability modeling of fractured reservoirs. *J Petrol Sci Eng*. 2011;77:326–37. doi:10.1016/j.petrol.2011.04.007.
- Rong YS, Li XH, Liu XL, et al. Discussion about the pattern of water flooding development in multi-well fractured-vuggy units of carbonate fracture-cavity reservoirs in the Tahe Oilfield. *Pet Geol Recovery Effic*. 2013;20(2):58–61 (in Chinese).
- Wang J, Liu HQ, Ning ZF, et al. Experiments on water flooding in fractured-vuggy cells in fractured-vuggy reservoirs. *Pet Explor Dev*. 2014;41(1):74–81 (in Chinese).
- Wu YS, Di Y, Kang ZJ, et al. A multiple-continuum model for simulating single-phase and multiphase flow in naturally fractured vuggy reservoirs. *J Pet Sci Eng*. 2011;78:13–22. doi:10.1016/j.petrol.2011.05.004.
- Xiao MH, Cao Y, Zhang XB, et al. The research on the ancient Karst of Ordovician reservoir in Block 4 of Tahe Oilfield. *Pet Geol Eng*. 2010;24(3):31–3 (in Chinese).
- Xu X, Tian SS, Xu T. The equivalent numerical simulation of fractured-vuggy carbonate reservoir. *Mech Aerosp Eng*. 2012;110–116:3327–31. doi:10.4028/www.scientific.net/AMM.110-116.3327.
- Xu X, Wei GQ, Yang ZM. The productivity calculation method of a carbonate reservoir. *Pet Sci Technol*. 2013;31(3):301–9. doi:10.1080/10916466.2010.525586.
- Yi B, Cui WB, Lu XB, et al. Analysis of dynamic connectivity of a carbonate reservoir with fractures and caves in the Tahe Field, Tarim Basin. *Xinjiang Pet Geol*. 2011;32(5):469–72 (in Chinese).
- Yousef AN, Behzad T, Abolghasem KR, et al. A combined Parzen-wevelet approach for detection of vuggy zones in fractured carbonate reservoirs using petrophysical logs. *J Petrol Sci Eng*. 2014;119:1–7. doi:10.1016/j.petrol.2014.04.016.
- Zhang D, Li AF, Yao J, et al. A single-phase fluid flow pattern in a kind of fractured-vuggy media. *Pet Sci Technol*. 2011;29(10):1030–40. doi:10.1080/10916466.2011.553657.
- Zhang K, Wang DR. Types of karst-fractured and porous reservoirs in China's carbonates and the nature of the Tahe Oilfield in the Tarim Basin. *Acta Geol Sinica*. 2004;78(3):866–72. doi:10.1111/j.1755-6724.2004.tb00208.x.
- Zhang P, Wen XH, Ge LZ, et al. Existence of flow barriers improve horizontal well production in bottom water reservoirs. In: SPE annual technical conference and exhibition, 21–24 September, Denver, Colorado, USA; 2008. doi:10.2118/115348-MS.
- Zheng XM, Sun L, Wang L, et al. Physical simulation of water displacing oil mechanism for vuggy fractured carbonate rock reservoirs. *J Southwest Pet Univ (Sci Technol Ed)*. 2010;32(2):89–92 (in Chinese).
- Zhu R, Lou ZH, Jin AM, et al. Fluid distribution and dynamic responses to exploitation in fracture-cave unit S48 in Tahe Oilfield. *J Zhejiang Univ (Eng Sci)*. 2009;43(7):1344–8 (in Chinese).
- Zuta J, Fjelle I. Mechanistic modeling of CO₂-foam processes in fractured chalk rock: effect of foam strength and gravity forces on oil recovery. In: SPE enhanced oil recovery conference, 19–21 July, Kuala Lumpur, Malaysia; 2011. doi:10.2118/144807-MS.